Phase diagram and spin-canting effects in electron-doped $LaMnO_3$

P. Schlottmann
Department of Physics, Florida State University, Tallahassee, Florida 32306, USA
(Received 18 June 2007; revised manuscript received 27 February 2008; published 31 March 2008)

In hole-doped $LaMnO_3$, i.e., La is partially substituted by Ca or Sr, the manganese ions are in a mixed-valent state of two magnetic configurations, Mn^{4+} (spin 3/2) and Mn^{3+} ($S=2$), while in electron-doped $LaMnO_3$, where La is partially replaced by Ce, the two mixed-valent configurations are Mn^{3+} and Mn^{2+} ($S^*=5/2$, half-filled shell). The Mn^{3+} configuration can be considered an e_g hole in the half-filled shell. The e_g holes are allowed to hop between the Mn sites with hopping amplitude t, but the multiple occupancy of the e_g levels is excluded at each site by a large Coulomb energy. This hopping of the e_g holes gives rise to the ferromagnetic double-exchange mechanism, which competes with the antiferromagnetic superexchange J between the localized spins S. By using a mean-field slave-boson formulation, we calculate the ground state energy of the system for the localized spins oriented in the magnetic configurations of the A, B, C, and G phases of $La_{1-y}Ce_yMnO_3$ as a function of y and one model parameter, J/t. Although the models are quite different, the phase diagram for electron doping is similar to that for hole doping. The effect of canting of the spins on the band structure of the itinerant e_g electrons and the stability of the A and B phases toward canting are discussed.

DOI: 10.1103/PhysRevB.77.104446 PACS number(s): 75.47.Lx, 75.47.Gk

I. INTRODUCTION

The rich phase diagram of $La_{1-x}R_xMnO_3$, where R is a divalent or tetravalent ion (e.g., Ca, Sr, or Ce), is a consequence of the interplay of charge, spin, orbital, and lattice degrees of freedom.[1–3] The partial substitution of trivalent La by divalent Ca or Sr corresponds to hole doping of $LaMnO_3$, while replacing La by tetravalent Ce gives rise to electron doping.[4] The range of these substitutions is limited by the tolerance factor [ratio of the distance between the cation and O ions and the MnO bond length divided by $\sqrt{2}$, i.e., $d_{R\text{-}O}/(\sqrt{2}d_{Mn\text{-}O})$]. Only for $La_{1-x}Ca_xMnO_3$ (LCMO) the tolerance factor is close to 1 and the alloy can form over the entire concentration range, $0 \leqslant x \leqslant 1$.[5,6] The end compounds of LCMO, $LaMnO_3$ and $CaMnO_3$, are antiferromagnetic insulators, while for intermediate x, the system is either a ferromagnetic metal or a charge-ordered antiferromagnet and may display phase separation.[7,8] The Jahn–Teller coupling to the lattice[9–11] changes the Mn-O-Mn bond lengths and angles[12] and gives rise to orbital order.[13] Electron-doped manganites (Ce-doping) have been less studied and are limited to less than 50% substitution by the tolerance factor.

In $La_{1-x}R_xMnO_3$, the Mn ions form a nearly simple cubic lattice with one oxygen ion located approximately on the center of each side and the La or R atoms at the body center of the cube. The O^{2-} ions mediate the binding between the Mn ions, while the role of La and R doping is to provide conduction electrons.[14] In cubic or nearly cubic symmetry, the five $3d$ levels are split into a t_{2g} triplet and an e_g doublet. With octahedral coordination, the t_{2g} states have lower energy than the e_g orbitals. For hole-doped systems, the Mn ions are in a mixed trivalent ($3d^4$) and tetravalent ($3d^3$) state, so that the three t_{2g} orbitals are all singly occupied with their spins coupled to form a total spin 3/2. The e_g orbitals, on the other hand, are empty for Mn^{4+} and occupied by one $3d$ electron in Mn^{3+}, ferromagnetically correlated with the t_{2g} electrons via the Hund's rule. The intermediate valence character of the Mn ions arises from the hopping of the e_g electrons. For electron doping, on the other hand, the Mn ions are in a mixed divalent ($3d^5$) and trivalent ($3d^4$) state. For Mn^{2+}, each of the five orbitals is singly occupied and all spins are ferromagnetically correlated to a total spin $S^*=5/2$. The trivalent ion has an e_g electron missing, so that the mixed valence character is induced by the itinerant e_g hole. The hole can be in either of the two e_g orbitals, but its spin is locally correlated with the spin of the localized electrons.

In a previous publication,[15] we studied hole-doped manganites as a cubic lattice of mixed-valent Mn ions with the t_{2g} spins (treated classically) oriented in the spin arrangements of the A, B, C, and G phases of the manganites.[5] The multiple occupancy of the e_g levels at each site is prevented by a large Coulomb interaction, which is taken into account with auxiliary bosons in the mean-field approximation. The e_g electrons are allowed to hop between nearest neighbor sites with amplitude t, which gives rise to the ferromagnetic double exchange.[16,17] We obtained the band structure for the e_g electrons and the ground state energy for each of the phases. For a given doping x, the phase diagram then only depends on one parameter, namely, J/t. Our calculation reproduces the sequence of phases of LCMO as a function of x for J/t of the order of a few percent.

These results have been extended to include the Jahn–Teller coupling to the lattice.[18] A Jahn–Teller distortion lifts the degeneracy of the e_g levels and changes the band structure. Due to their anisotropic spin configurations, the A and C phases have an energy gain due to lattice distortions and, consequently, the region of stability of these phases grows at the expense of the B and G phases. The Jahn–Teller distortion consists of a compression (expansion) of the c axis for the A phase (C phase),[18] which is in agreement with experiments.[5,19] Further extensions of this calculation involve instabilities toward the canting of spins and long-range orbital order in the A phase.[20–22]

In this paper, we study the case of electron doping, i.e., $La_{1-y}Ce_yMnO_3$. Our hole-doping model is limited to one e_g

 ©2008 The American Physical Society

electron per site by the excluded multiple occupancy of every site. To overcome this restriction, it is necessary to allow the double occupancy of the Mn sites. Within the framework of slave bosons, this can be accomplished by enhancing the space of slave bosons similar to that of the Kotliar–Ruckenstein formalism[23,24] for the Hubbard model. This requires four bosons (two e_g orbitals times spin) for the Mn^{3+} configuration and six slave bosons for the Mn^{2+} configuration subject to Hund's rules. In mean field, the energy would have to be minimized with respect to all the parameters. A more practicable approach is to assume that e_g holes (at most one per site) are moving in the background of a Mn^{2+} lattice (half-filled $3d$ shells with spin $S^*=5/2$). Then only one slave boson (representing the charge of the e_g holes) is needed[25] and the approach has similarities with the hole-doped case. Both models, hole doping and electron doping, are physically quite different and have $LaMnO_3$ as the only common point. Since $LaMnO_3$ is an orbitally ordered insulator, there are difficulties in matching both models at that point. The present model is then not just an extension of the hole-doping model to a different range of parameters. The phase diagram for the electron- and hole-doping cases are very similar, which is in agreement with the experimental situation. This is different from the cuprates, where electron and hole doping lead to quite different results.

The rest of the paper is organized as follows. In Sec. II, the model for quasicubic electron-doped manganites is introduced. In Sec. III, we obtain the band structure for the e_g holes in the dominating B phase and the ground state phase diagram for electron doping. In Sec. IV, we analyze the consequences of the canting of the spins in the A and B phases. A discussion of the different classes of models for manganites is presented in Sec. V. Concluding remarks follow in Sec. VI.

II. MODEL

The Hamiltonian for electron-doped manganites can be written as $H=H_t+H_m$, where H_t represents the hopping of the e_g holes between the Mn^{2+} (half-filled shell) sites on a simple cubic lattice, and H_m is the magnetic energy arising from the superexchange between the localized spins S.

The nearest neighbor hopping Hamiltonian for the e_g holes is given by

$$H_t = \mu \sum_{jMm} |jSMm\rangle\langle jSMm| - t \sum_{\langle jl\rangle m_j m_l \sigma M_j M_l M_j^* M_l^*} \left(SM_j, \frac{1}{2}\sigma | S\frac{1}{2} S^* M_j^*\right) \times \left(SM_l, \frac{1}{2}\sigma | S\frac{1}{2} S^* M_l^*\right) \{ |jSM_j m_j\rangle\langle jS^* M_j^*| \hat{M}_{m_j m_l}(\mathbf{R}_{jl}) \times |lS^* M_l^*\rangle\langle lSM_l m_l| + \text{H.c.}\}. \quad (1)$$

Here, the bra and ket denote the states of the Mn ions at the sites labeled by j and l forming a simple cubic lattice, and $\langle jl\rangle$ denotes nearest neighbor sites. The states of the Mn^{2+} configuration are represented by a spin $S^*=5/2$ (half-filled $3d$ shell) and z projection M^*, while the states of the Mn^{3+} configuration by a spin $S=2$ and spin projection M. The localized $3d$ electrons are then all ferromagnetically correlated (Hund's rules). The Clebsch–Gordan coefficients select the spin components and are needed to preserve the spin rotational invariance. The index $m=x^2-y^2, z^2$ labels the e_g orbitals. The Mn^{3+} states have a label m to indicate which of the e_g states is empty ($3d$ hole). The completeness condition for the states requires that at every site

$$\sum_{Mm} |jSMm\rangle\langle jSMm| + \sum_{M^*} |jS^*M^*\rangle\langle jS^*M^*| = 1, \quad (2)$$

which excludes the multiple occupancy of the e_g holes, i.e., the shell can only be half-filled (no hole) or have at most one e_g hole. This corresponds to an implicit infinite Coulomb repulsion.

The first term in Eq. (1) determines the Fermi energy or chemical potential μ for the itinerant holes, while the second term corresponds to the nearest neighbor intersite hopping. The sum is over all the nearest neighbor pairs and σ is the spin component of the itinerant e_g hole. The hopping matrix $\hat{M}_{m_j m_l}(\mathbf{R}_{jl})$ depends on the direction of $\mathbf{R}_{jl}$, which can be along the x, y, or z directions. The corresponding matrices are

$$\hat{M}_x = \frac{1}{4}(2\hat{I} + \hat{\tau}_z + \sqrt{3}\hat{\tau}_x),$$

$$\hat{M}_y = \frac{1}{4}(2\hat{I} + \hat{\tau}_z - \sqrt{3}\hat{\tau}_x),$$

$$\hat{M}_z = \frac{1}{2}(\hat{I} - \hat{\tau}_z), \quad (3)$$

where $\hat{I}$ and $\hat{\tau}_i$ are the identity and Pauli matrices for the orbital pseudospin of components (x^2-y^2, z^2). These hopping matrices are determined by the overlap of the asymptotic of the e_g wave functions. The fact that x^2-y^2 and z^2 orbitals on neighboring sites have, in general, nonzero overlap implies that m is not a good quantum number.

We introduce slave-boson creation and annihilation operators,[25,26] $b_{jM^*}^\dagger$ and b_{jM^*}, which act as projectors onto the states of the Mn^{2+} configuration with spin component M^* at site j, and fermion operators for the Mn^{3+} states at the site j, with $d_{jMm}^\dagger$ and d_{jMm} representing the e_g holes. The completeness relation equivalent to the condition (2) is now[25,26]

$$\sum_{M^*} b_{jM^*}^\dagger b_{jM^*} + \sum_{Mm} d_{jMm}^\dagger d_{jMm} = 1. \quad (4)$$

Transitions between configurations are described by the operators $|jS^*M^*\rangle\langle jSMm| = b_{jM^*}^\dagger d_{jMm}$. The hopping Hamiltonian can now be rewritten in auxiliary space, subject to the constraint (4), which is incorporated via a Lagrange multiplier λ. The Hamiltonian in auxiliary space is completely equivalent to Eq. (1).

The magnetic interactions between neighboring localized Mn moments is of the antiferromagnetic superexchange type mediated by the O ions. The magnetic energy H_m depends on

the spin configuration of each phase. We consider four different spin arrangements corresponding to the phases A, B, C, and G.[5] The broken symmetry makes it more meaningful to incorporate the superexchange as $H_m=-\alpha JS^2N$, where $\alpha_A=-1$, $\alpha_B=-3$, $\alpha_C=+1$, and $\alpha_G=+3$, rather than as a spin-spin interaction of the Heisenberg type. Here, N is the number of Mn sites. The coupling strength J can be estimated from the transition temperature of the end compound $LaMnO_3$ and should be of the order of 100 times smaller than the hopping t.

The spin projections $M_j=\pm S$ of the localized moments are then determined by the magnetic phase of the system. The spin component σ of the itinerant e_g holes is now a good quantum number. The spin projection of the Mn^{2+} configuration is $M^*_j=\pm S+\sigma$. Only two cases have to be considered:[27] (i) If σ and M_j are parallel, the Clebsch–Gordan coefficient is equal to 1, while (ii) if they are antiparallel, the coefficient is $1/\sqrt{2S+1}$. We denote these coefficients $a_{j\sigma}$.

As for hole doping in Ref. 15, we study the present model for electron doping in the mean-field approximation. The boson operators are replaced by their expectation values,[26] i.e., $\langle b_{jM^*}\rangle=\langle b^\dagger_{jM^*}\rangle=b$ for $M^*=S$ or $M^*=-S$, depending on the magnetic configuration, and all others are zero. We can rewrite the fermion operators as $d^\dagger_{j\sigma m}$ and $d_{j\sigma m}$ and the mean-field Hamiltonian is

$$H_{mf}=(\mu-\lambda)\sum_{j\sigma m} d^\dagger_{j\sigma m}d_{j\sigma m}+N\lambda(1-b^2)$$
$$+tb^2\sum_{\langle jl\rangle\sigma m_j m_l} a_{j\sigma}a_{l\sigma}\{d^\dagger_{j\sigma m_j}\hat{M}_{m_j m_l}(\mathbf{R}_{jl})d_{l\sigma m_l}+\text{H.c.}\}$$
$$-\alpha JS^2N. \tag{5}$$

By Fourier transforming H_{mf}, we obtain the band structure for the e_g holes, which, of course, depends on the magnetic phase. In all four phases, there are four bands with generally different dispersions, which arise from the two e_g orbitals and the two sites per unit cell. In the case of the B phase, they arise from the two e_g levels and the spin. Although the four phases have different magnetic unit cells, we adopt the simple cubic Brillouin zone to facilitate a direct comparison between all phases.

The ground state expectation value of H_{mf} is to be minimized with respect to b and λ, yielding

$$b^2=y=1-\frac{1}{N}\sum_{\mathbf{k}\alpha}\{1-f[\lambda-\mu+E^t_\alpha(\mathbf{k})]\}, \tag{6}$$

$$\lambda=-\frac{1}{Nb^2}\sum_{\mathbf{k}\alpha}E^t_\alpha(\mathbf{k})\{1-f[\lambda-\mu+E^t_\alpha(\mathbf{k})]\}, \tag{7}$$

where $E^t_\alpha(\mathbf{k})$, $\alpha=1,\ldots,4$, are the band energies, f is the Fermi function, and the sum is over the simple cubic Brillouin zone. The spin degeneracy is already incorporated in the sums. Here, $1-y$ is the fraction of e_g holes in the half-filled f shell. The ground state energy per Mn ion is given by

$$E_{GS}/N=[\lambda y+\mu(1-y)-4J\alpha]. \tag{8}$$

At a first glance, the Hamiltonian (1) for electron-doped manganites resembles the one for hole doping,[15] i.e., for LCMO. There are, however, some dramatic differences. (1) In the present case, the hole states are filled from the top of the bands, while the electron states in Ref. 15 are filled from the bottom of the bands. (2) In both cases, the compound $LaMnO_3$ corresponds then to quarter-filling. This is the only overlap point of the two models. However, due to the orbital long-range order in $LaMnO_3$, there are additional band splittings and the compound is actually an insulator. (3) It is possible to stress the analogies and differences between the two models further, by defining the following particle-hole transformation:

$$d^\dagger_{j\sigma m}\rightarrow e^{i\pi(n_{jx}+n_{jy}+n_{jz})}c_{j\sigma m},$$
$$d_{j\sigma m}\rightarrow c^\dagger_{j\sigma m}e^{-i\pi(n_{jx}+n_{jy}+n_{jz})}, \tag{9}$$

where n_{jx} is the projection of the Mn position vector $\mathbf{R}_j$ onto the x axis in units of the lattice constant a. This transformation converts hole states into particle states. In view of the implicit infinite Coulomb repulsion, the particle states, however, do not correspond to electrons. In terms of the c operators, the hopping Hamiltonian has now the same form as the one for hole doping.[15] (4) After this transformation, the two models are still not the same, because the completeness condition also changes and the constraint is no longer the same. (5) The fact that we cannot exactly map the two models onto each other is a direct consequence of the large Coulomb repulsion.

In summary, the present model is not the continuation of that of Ref. 15 to a different parameter range, but a different model. The two models, however, have similarities, so that the results are also expected to be related.

III. BAND STRUCTURE AND PHASE DIAGRAM

Due to the magnetic order of the A and C phases, the x, y, and z directions in the cubic Brillouin zone are generally not equivalent. The band structure shown below is along the following directions: From Γ (body center of the cube) to X (center of the face) along $\mathbf{k}=(k_x,0,0)$, then from X to M (middle of a side) varying k_y from 0 to π along $(\pi,k_y,0)$, from M to R (corner of the cube) along (π,π,k_z), from R to Γ along $(k/\sqrt{3})(1,1,1)$, and from Γ to M along $(k/\sqrt{2})(1,1,0)$. Finally, X to R refers to the line $(\pi,k/\sqrt{2},k/\sqrt{2})$.

In the A phase, the localized spins are ferromagnetically oriented in x-y planes and these planes are antiferromagnetically correlated along the z direction. In the B phase, all localized spins are ferromagnetically correlated, while the C phase consists of ferromagnetic chains along the z direction, which are antiferromagnetically correlated to each other in the x-y plane. In the G phase, each up spin is surrounded by neighbors with down spins and vice versa.

The band structure of the e_g holes in the B phase is shown in Fig. 1. Since this phase is ferromagnetic, the unit cell contains only one Mn ion. Due to the $a_{j\sigma}$ coefficients, the band for e_g holes with spin parallel to the localized spins is

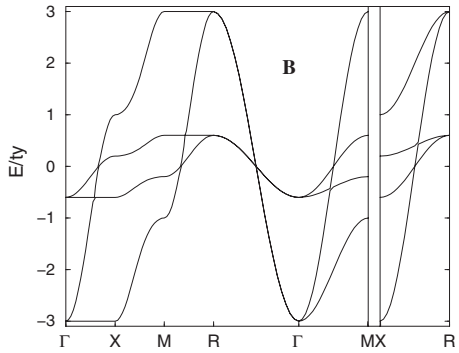

FIG. 1. Band structure for the ferromagnetic B phase within the simple cubic Brillouin zone, with the energy normalized to ty. The dispersion for the holes with polarization opposite to the magnetization is five times smaller than that parallel to the localized moments.

$(2S+1)=5$ times more dispersive than the one for antiparallel e_g spins. This gives rise to the ferromagnetic double-exchange mechanism. The four bands arise from the two e_g orbitals of each Mn ion and the two spin components. According to Eqs. (6) and (7), the e_g holes are filled from the top of the bands, so that the bands are completely filled ($y=1$) for $CeMnO_3$, and there is one e_g hole per Mn ion for $LaMnO_3$ ($y=0$). These states have a spin polarization parallel to that of the localized spins, so that the total magnetization per Mn ion increases with increasing y. This is opposite to what happens with Ca (Sr) doping. The magnetization has then a localized and an itinerant component. Note that in the ferromagnetic B phase the hopping is isotropic.

The band structure of the e_g holes in the A phase is shown by the solid curves in Fig. 2. Since the localized spins in the x-y planes are ferromagnetically correlated, the motion of the e_g holes is predominantly in these planes. The magnetic unit cell consists of two sites, one with localized up-spin and one with localized down-spin. Both spin directions of the e_g holes give rise to the same band dispersion. The four bands arise from the two Mn ions per unit cell and the two e_g

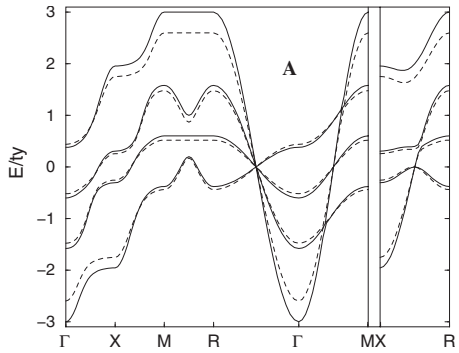

FIG. 2. Band structure for the magnetic A phase within the simple cubic Brillouin zone with the energy normalized to ty. The four bands arise from the two sites within the magnetic unit cell and two e_g orbitals per Mn. The solid lines correspond to the bands for the magnetic configuration of the A phase, and the dashed curves to a canting of the spins by $\pi/3$ in the x-y plane.

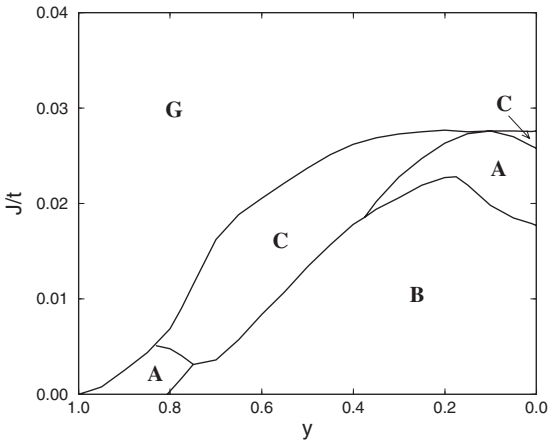

FIG. 3. Phase diagram for electron doping obtained by comparing the ground state energies of the four phases A, B, C, and G as a function of J/t and y.

orbitals. The total bandwidth is $6ty$. Again, the e_g holes are filled from the top of the bands. The dashed curves refer to the localized moments canted by $\pi/3$ in the x-y plane and are discussed in Sec. IV.

The phase diagram is obtained by comparing the ground state energies of the four phases for a given y. First, the hard-core parameter $\lambda-\mu$ is determined by solving Eq. (6). Then the value of λ is obtained from Eq. (7) and, finally, the ground state energy is determined for each phase. For a given y, E_{GS}, when normalized to the hopping t, is a function of only one dimensionless model parameter, namely, J/t.

Several energy crossovers are obtained for a fixed y as a function of the superexchange coupling J. The boundaries of the phases of lowest energy are shown in Fig. 3. For sufficiently large J, the G phase is always the ground state, since it has all antiferromagnetic bonds and, hence, the lowest magnetic energy. The ferromagnetic B phase is favored at most values of y for small J. The ferromagnetism is rapidly quenched by the antiferromagnetic superexchange J. The A and C phases are intermediate phases between the ferromagnetic B phase and the totally antiferromagnetic G phase.

The band structure for the electron-doped manganites is very similar (but not identical) to the one of the hole-doped manganites. This analogy, however, is only superficial, because the models for the two cases are rather different. The key difference is that for hole doping, the two configurations of Mn are the trivalent and tetravalent ones, while for electron doping, Mn is intermediate valent between divalence and trivalence. Hence, in the hole-doped situation, the bands are populated with electrons starting from the bottom of the bands (the Γ point), while in the electron-doped case, the bands are populated with holes from the top of the bands. Although the band structure is not invariant under a change of sign of t, the total energy only depends on $|t|$ but not on its sign.

At a first glance, the phase diagram shown in Fig. 3 for electron doping is a mirror image of Fig. 5(a) in Ref. 15 corresponding to hole doping. A more detailed comparison, however, reveals that there are differences arising from the fact that the localized spins of the higher-valent electronic

configuration are different, i.e., $S=3/2$ and $S=2$, respectively. This affects the magnetic energy as well as the Clebsch–Gordan coefficient for carrier spin opposite to the localized one, $a=1/\sqrt{2S+1}$.

In the limit $x\to 0$ and $y\to 0$, both models lead to the limiting case $LaMnO_3$. In both cases, the bandwidth becomes very small as a consequence of the excluded multiple occupancy of the sites. In this limit, the A and B phases compete and the energy is determined by the hard-core potential (Lagrange multiplier λ). This parameter is not the same on both sides of the phase diagram (electron and hole doping), because the spins are different, e.g., in the A phase, the motion of e_g holes is "more two-dimensional" than that of e_g electrons.

IV. CANTING OF LOCALIZED SPINS

The magnetic energy H_m and the effective hopping are modified when the localized spins are not perfectly parallel or antiparallel to each other. Let us denote the canting angles at site j with θ_j and ϕ_j. The hopping between neighboring sites j and l is then given by[28,29]

$$t \to t\{\cos(\theta_j/2)\cos(\theta_l/2) + \sin(\theta_j/2)\sin(\theta_l/2)\exp[-i(\phi_j - \phi_l)]\}. \tag{10}$$

If we exclude spin-spiral states and Berry phases, this expression can be simplified by choosing $\phi_j=\phi_l$, so that the effective hopping is $t\cos[(\theta_j-\theta_l)/2]$. In addition, if canting gives rise to two sublattices, we may write $\theta_j=-\theta_l=\theta_{jl}/2$ and have $t\cos(\theta_{jl}/2)$ for the canting of the localized spin at that bond.[30] We assume that the θ_{jl} are small and, for simplicity, we distinguish between θ_z (along the z axis) and θ_{xy} within the x-y plane.[31]

Since the canting affects the hopping of the e_g holes, also the band structure is changed. This is shown for the A phase with $\theta_{xy}=\pi/3$ and $\theta_z=0$ by the dashed curves in Fig. 3. Since the hopping matrix element is effectively reduced by the canting, the overall bandwidth has decreased.

In terms of the canting angles, the coefficient α of the magnetic energy H_m for the A, B, C, and G phases is given by[20,31] $\alpha_A=-2\cos(\theta_{xy})+\cos(\theta_z)$, $\alpha_B=-2\cos(\theta_{xy})-\cos(\theta_z)$, $\alpha_C=2\cos(\theta_{xy})-\cos(\theta_z)$, and $\alpha_G=2\cos(\theta_{xy})+\cos(\theta_z)$.

The total energy now has to be minimized as well with respect to θ_{xy} and θ_z. Consider first the magnetic energy. If the bond is antiferromagnetic, the contribution to H_m is minimum if θ is zero. On the other hand, if the bond is ferromagnetic, magnetic energy is gained by canting the localized spins. The energy gain is proportional to $1-\cos(\theta/2)^2$. The canting of the spins almost always increases the hopping energy, E_t, with a linear dependence on $\cos(\theta/2)$ for small angles. Hence, minimizing the total energy for given y in a given phase yields

$$\beta = \left.\frac{\partial E_t/N}{\partial\cos(\theta/2)}\right|_{\theta=0} = \pm 4dJS^2\cos\left(\frac{\theta}{2}\right), \tag{11}$$

where the plus (minus) sign corresponds to the ferromagnetic (antiferromagnetic) bond, and $d=1$ for θ_z and $d=2$ for θ_{xy}.[20]

The y dependence of the derivative of the hopping energy with respect to $\cos(\theta/2)$, β_{xy} and β_z, is displayed in Fig. 4 for the A phase. β_z is a positive quantity for all y except for rather large y, where the A phase is no longer stable (see Fig. 3). Hence, the minimum of the energy corresponds to $\theta_z=0$, since the bonds along the z axis are antiferromagnetic. Canting within the x-y plane is achieved if Eq. (11) is satisfied for θ_{xy}. This is only the case for relatively large values of the superexchange J. These results are similar to those obtained for the A phase of hole-doped manganites.

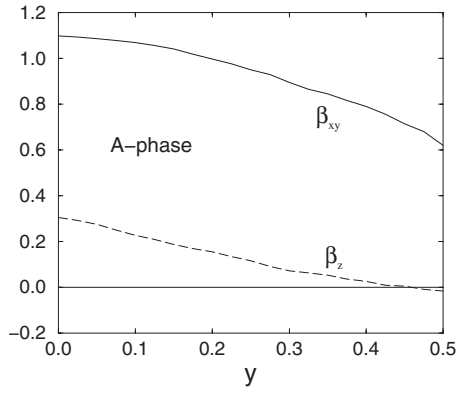

FIG. 4. The derivative of the hopping energy (in units of t) in the A phase with respect to $\cos(\theta/2)$, as defined in Eq. (11) as a function of y. The solid line corresponds to canting in the x-y plane, and the dashed curve to tilting along the z axis.

In Fig. 5, we present the results corresponding to the B phase. All bonds are ferromagnetic now and one expects that $\beta_{xy}\approx 2\beta_z$. Again, canting in the B phase can only be realized for rather large values of J. The G phase, on the other hand, is isotropic with all bonds being antiferromagnetic, so that no instability toward canting is obtained.

When two phases, e.g., the A and B phases, have about the same energy, i.e., close to the phase boundary, there is a tendency to phase separate.[7] Small inhomogeneities in y can then locally favor one phase over the other. The canting instabilities help the formation of domain walls separating the phases and are then instrumental for the phase separation to be implemented.

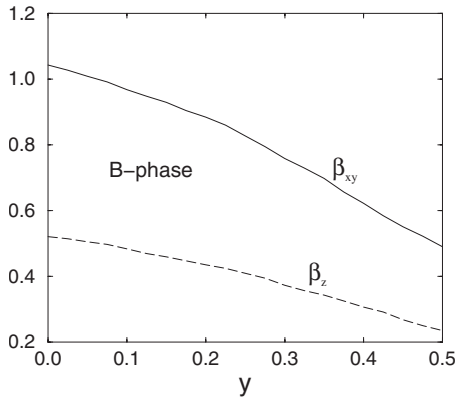

FIG. 5. The derivative of the hopping energy (in units of t) in the B phase with respect to $\cos(\theta/2)$, as defined in Eq. (11) as a function of y. The solid line corresponds to canting in the x-y plane, and the dashed curve to tilting along the z axis.

V. DISCUSSION

Models for manganites broadly belong into one of two categories: (1) models with a large on-site Hubbard repulsion between the e_g electrons (or holes) and (2) models that are based on a strong Jahn–Teller coupling.

A Coulomb interaction of several electron volts is always present in the $3d$ shell of transition metal ions. In the present case, the repulsion prevents the occupation of electronic configurations of Mn other than the divalent and the trivalent. The characteristic energy of the phonons (e.g., the Debye temperature) is much weaker and of the order of a few hundreds of eV. It is then expected that the Jahn–Teller energy for the coupling of the e_g electrons (holes) to the lattice does not exceed a tenth of an eV. In other words, it is much weaker than the Coulomb energy and also smaller than the hopping integral t. This effect is sufficient to explain partially the compression (stretching) of the c axis in the A phase (C phase) and the orbital long-range order in the A phase. While the magnitude of the change of the c axis (deviation from a cube) is much smaller than the measured value (electronic energies possibly play a role here), the energy of the orbital order appears to have the correct order of magnitude. So far, we have ignored the CE phase, which involves charge order. Charge order can be driven either by a nearest neighbor Coulomb repulsion or the Jahn–Teller effect induced by the A_{1g} breathing mode, which alternatingly have to expand and contract the MnO_6 octahedra. In the present slave-boson formulation, charge order requires two sets of slave-boson expectation values and two sets of Lagrange multipliers for the completeness condition.

Models of class (2) require a strong Jahn–Teller coupling, in addition to a strong Hund's rule coupling of the spins.[2,32] A large distortion of the octahedra leads to a crystalline electric field splitting of the e_g levels, lifting their degeneracy. Hence, only one e_g level can have a significant occupation. These models are then, to some extent, equivalent to approaches where the orbital e_g degrees of freedom are neglected. The effect of the crystalline field is then similar to that of a large Coulomb repulsion. This picture is clear for the A and C phases, where due to the anisotropic spin arrangements the hopping is anisotropic and supports a Jahn–Teller distortion. However, for the isotropic B and G phases, a Jahn–Teller distortion does not occur (there is, however, magnetostriction) and, as a consequence, other Mn electronic configurations than the two dominant ones (in the present case, divalent and trivalent) will have a significant population. This would violate the generally accepted assumptions for the valence states of Mn.[14] Hence, it makes a difference if Coulomb interactions or a strong Jahn–Teller effect are considered. On the other hand, charge and orbital order can be incorporated quite naturally within the Jahn–Teller formalism.

Phase separation is a prominent feature in manganites.[7,8] In strongly correlated models, phase separation appears in calculations carried out at constant chemical potential. This is not the case in the present paper, because the chemical potential is determined for a fixed density of e_g carriers. Phase separation can also occur due to inhomogeneities in the sample. Phase separation is expected to occur in the neighborhood of phase boundaries, where two phases have very comparable energies. Working against phase separation is the surface energy separating the phases (domain boundary).[8] Inhomogeneities, as a consequence of doping, can give rise to local canting of the localized spins, which facilitates the formation of narrow domain walls separating the phases.

VI. CONCLUDING REMARKS

We considered a simple cubic lattice of Mn ions in an intermediate valence state between two magnetic configurations, Mn^{2+} and Mn^{3+}. The Mn^{2+} configuration has a half-filled $3d$ shell with a total spin $S^*=5/2$, whereas the Mn^{3+} configuration has been represented by the half-filled shell and a hole in one of the e_g orbitals with a total spin $S=2$. The e_g hole is itinerant and can move throughout the lattice with directed hopping subject to excluded multiple occupation (large Coulomb potential) and Hund's rules maximizing the spin at every site. The localized spins interact with each other via a nearest neighbor superexchange, which competes with the double exchange caused by the hopping of the e_g holes. This model contains all the important ingredients to describe electron-doped manganites.

The hopping of the e_g holes depends on the orbital (x^2-y^2 or z^2) and on the magnetic order of the localized spins of the phase under consideration. The excluded multiple occupation of the e_g holes at each site is taken into account via slave bosons in the saddle point approximation. The phase diagram for electron-doped manganites is obtained by comparing the energies of the A, B, C, and G phases for each y and J/t. Here, we exclude the CE phase, which in addition to spin order also has charge order and requires a larger unit cell. The phase diagram as a function of y is approximately the mirror image of the phase diagram for hole-doped manganites as a function of x. The former qualitatively agrees with the observed phases in $La_{1-y}Ce_yMnO_3$ and the latter reproduces the experimental sequence of phases in $La_{1-x}Ca_xMnO_3$.[15]

For electron-doped manganites, i.e., the substitution of trivalent La in $LaMnO_3$ by tetravalent Ce is limited by the tolerance factor to doping concentrations y less than 0.5. In this region of the phase diagram, the ferromagnetic B phase dominates.[4,33] Note that the strength of the superexchange is not the same for electron doping and hole doping. Although the localized spin is larger for electron doping, the coupling constant is weaker, because the energy required for the virtual electron transfer process to the O ion leading to the superexchange is larger. Hence, the A phase can only play a role for very small y. For $y\to 0$, the A phase is insulating, as a consequence of the long-range orbital order (not considered here). For small y, one band is then almost empty and disorder leads to localization of the e_g electrons, such that we are actually in the presence of a ferromagnetic insulator, as experimentally observed for Ce doping.[33]

In this paper, we also investigated a possible canting of the localized moments. We limited ourselves to the relevant regime, i.e., the A and B phases for $y\leqslant 0.5$. Canting between localized spins is likely along directions with ferromagnetic

bonds. For electron doping, canting is possible within the x-y planes in the A phase, however, only for relatively large values of J/t. The B phase, where all localized spins are ferromagnetically coupled, is unstable to canting, but again only for unphysically large values of J/t.

A tetravalent cation may change the local environment, i.e., by distorting the MnO_6 octahedra in the neighborhood (Jahn–Teller effect). This lifts the degeneracy of the e_g hole levels. The band structure is then spread over a larger energy interval, and changes in the hopping amplitude through $\cos(\theta_{xy}/2)$ and $\cos(\theta_z/2)$ will affect $\langle H_t \rangle$ less than in the degenerate case. Consequently, β_{xy} and β_z are locally smaller than those calculated, and more modest values of J/t will lead to local canting.[30] Two phases that are energetically nearly degenerate (close to the phase boundary) may phase separate. The canting instabilities of local moments can then lead to the formation of domain walls (separating the phases) and, hence open the door to phase separation.

ACKNOWLEDGMENT

The support by the U.S. Department of Energy under Grant No. DE-FG02-98ER45707 is acknowledged.

[1] *Physics of Manganites*, edited by T. A. Kaplan and S. D. Mahanti (Kluwer Academic, Dordrecht Plenum, New York, 1999).
[2] E. Dagotto, T. Hotta, and A. Moreo, Phys. Rep. **344**, 1 (2001).
[3] M. B. Salamon and M. Jaime, Rev. Mod. Phys. **73**, 583 (2001).
[4] C. Mitra, P. Raychaudhuri, J. John, S. K. Dhar, A. K. Nigam, and R. Pinto, J. Appl. Phys. **89**, 524 (2001).
[5] E. O. Wollan and W. C. Koehler, Phys. Rev. **100**, 545 (1955).
[6] R. von Helmolt, J. Wecker, B. Holzapfel, L. Schultz, and K. Samwer, Phys. Rev. Lett. **71**, 2331 (1993); K. Chahara, T. Ohuo, M. Kasai, and Y. Kozono, Appl. Phys. Lett. **63**, 1990 (1993); G. C. Xiong, Q. Li, H. L. Ju, S. N. Mao, L. Senapathi, X. X. Xi, R. L. Greene, and T. Venkatesan, *ibid.* **66**, 1427 (1995); Y. Tokura, A. Urishibara, Y. Moritomo, T. Arima, A. Asamitsu, G. Kido, and N. Furukawa, J. Phys. Soc. Jpn. **63**, 3931 (1994).
[7] S. Yunoki, J. Hu, A. L. Malvezzi, A. Moreo, N. Furukawa, and E. Dagotto, Phys. Rev. Lett. **80**, 845 (1998); A. Moreo, S. Yunoki, and E. Dagotto, Science **283**, 2034 (1999); L. P. Gor'kov and V. Z. Kresin, J. Supercond. **12**, 243 (1999).
[8] P. Schlottmann, Phys. Rev. B **59**, 11484 (1999).
[9] G. Zhao, K. Conder, H. Keller, and K. A. Müller, Nature (London) **381**, 676 (1996).
[10] A. J. Millis, B. I. Shraiman, and R. Mueller, Phys. Rev. Lett. **77**, 175 (1996); Z. Popović and S. Satpathy, *ibid.* **88**, 197201 (2002); T. V. Ramakrishnan, H. R. Krishnamurthy, S. R. Hassan, and G. Venketeswara Pai, *ibid.* **92**, 157203 (2004).
[11] G. J. Snyder, R. Hiskes, S. DiCarolis, M. R. Beasley, and T. H. Geballe, Phys. Rev. B **53**, 14434 (1996).
[12] C. H. Booth, F. Bridges, G. J. Snyder, and T. H. Geballe, Phys. Rev. B **54**, R15606 (1996); S. J. L. Billinge, R. G. DiFrancesco, G. H. Kwei, J. J. Neumeier, and J. D. Thompson, Phys. Rev. Lett. **77**, 715 (1996).
[13] B. B. Van Aken, O. D. Jurchescu, A. Meetsma, Y. Tomioka, Y. Tokura, and T. T. M. Palstra, Phys. Rev. Lett. **90**, 066403 (2003); M. C. Sánchez, G. Subías, J. García, and J. Blasco, *ibid.* **90**, 045503 (2003); X. Qiu, Th. Proffen, J. F. Mitchell, and S. J. L. Billinge, *ibid.* **94**, 177203 (2005).
[14] J. Goodenough, Phys. Rev. **100**, 564 (1955).
[15] P. Schlottmann, Phys. Rev. B **62**, 439 (2000).
[16] C. Zener, Phys. Rev. **82**, 403 (1951); P. W. Anderson and H. Hasegawa, *ibid.* **100**, 675 (1955).
[17] A. J. Millis, P. B. Littlewood, and B. I. Shraiman, Phys. Rev. Lett. **74**, 5144 (1995); N. Furukawa, J. Phys. Soc. Jpn. **64**, 2734 (1995); H. Röder, Jun Zang, and A. R. Bishop, Phys. Rev. Lett. **76**, 1356 (1996).
[18] P. Schlottmann, Phys. Rev. B **73**, 214428 (2006).
[19] Q. Huang, A. Santoro, J. W. Lynn, R. W. Erwin, J. A. Borchers, J. L. Peng, K. Ghosh, and R. L. Greene, Phys. Rev. B **58**, 2684 (1998).
[20] P. Schlottmann, IEEE Trans. Magn. **43**, 3085 (2007).
[21] P. Schlottmann, Physica B **384**, 187 (2006).
[22] P. Schlottmann, Physica B **403**, 1642 (2008).
[23] G. Kotliar and A. E. Ruckenstein, Phys. Rev. Lett. **57**, 1362 (1986).
[24] V. Dorin and P. Schlottmann, Phys. Rev. B **47**, 5095 (1993).
[25] S. E. Barnes, J. Phys. F: Met. Phys. **6**, 1375 (1976); P. Coleman, Phys. Rev. B **29**, 3035 (1984).
[26] N. Read and D. M. Newns, J. Phys. C **16**, L1055 (1983).
[27] P. Schlottmann, Phys. Rev. B **60**, 7911 (1999).
[28] I. V. Solovyev and K. Terakura, Phys. Rev. B **63**, 174425 (2001).
[29] T. Ohsawa and J. I. Inoue, Phys. Rev. B **65**, 134442 (2002).
[30] P. G. de Gennes, Phys. Rev. **118**, 141 (1960).
[31] J. van den Brink and D. Khomskii, Phys. Rev. Lett. **82**, 1016 (1999).
[32] J. L. Alonso, J. A. Capitán, L. A. Fernández, F. Guinea, and V. Martín-Mayor, Phys. Rev. B **64**, 054408 (2001).
[33] C. Mitra, P. Raychaudhuri, K. Dörr, K.-H. Müller, L. Schultz, P. M. Oppeneer, and S. Wirth, Phys. Rev. Lett. **90**, 017202 (2003); P. Raychaudhuri, C. Mitra, P. D. A. Mann, and S. Wirth, J. Appl. Phys. **93**, 8328 (2003); C. Mitra, Z. Hu, P. Raychaudhuri, S. Wirth, S. I. Csiszar, H. H. Hsieh, H.-J. Lin, C. T. Chen, and L. H. Tjeng, Phys. Rev. B **67**, 092404 (2003).